Multidimensional slope limiters for MUSCL-type finite volume schemes *

M.E.Hubbard

The University of Reading, Department of Mathematics,

P.O.Box 220, Whiteknights, Reading, Berkshire, RG6 6AX, U.K.

30th March 1998

Abstract

A number of multidimensional slope limiting operators are presented for MUSCL-type finite volume schemes in two dimensions on triangular grids. The most compressive limiter considered, in the sense that it attains the highest possible magnitude for their constructed solution gradient, is implemented in a manner higher by their construction of the solution

1 Introduction

High order Total Variation Diminishing (TVD) schemes hav

of equations, specifically the shallo

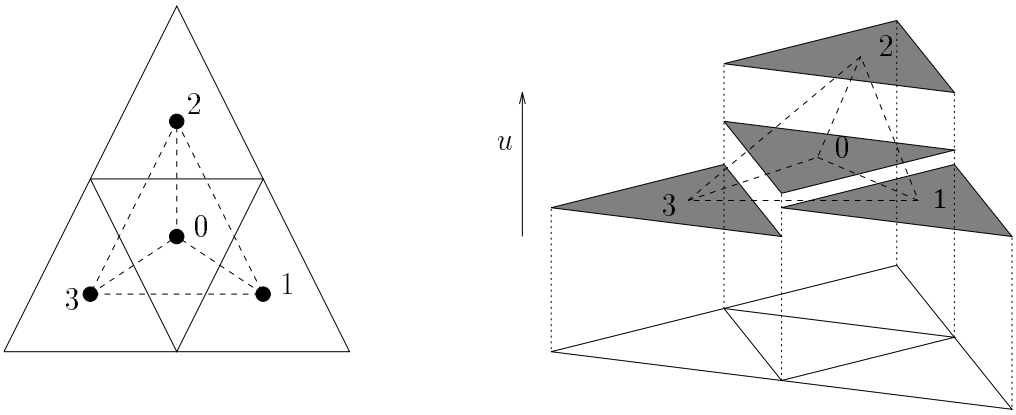

Figure 2.1: The limiting planes atriangularcon

2.1 Gradien

In the present case the numerical flux function of Equation (2.6) at a cell edge, such as one of those shown in Figure 2.2, is written in terms of the reconstructed solution values from the two neighbouring cells at the midpoint of the edge, so that $\vec{f}^*$ is now written

$$\vec{f}^*(u_L, u_R) \;=\; \vec{f}^*(u_0 + \vec{r}_{0k} \cdot \vec{L}_0,\; u_k + \vec{r}_{k0} \cdot \vec{L}_k) \;, \tag{2.9}$$

where $\vec{r}_{ij}$ is the vector from the centroid of cell i to the midpoint of the edge between cells i and j, and $\vec{L}_i$ is the gradient of the reconstructed solution in cell i. In the notation used here u_L is considered to be an *interior* reconstructed solution value relative to the cell under consideration and u_R is the corresponding *exterior* value, taken from the adjacent cellwhich is generally different. This motivates the subsequent use of a Riemann solver to evaluate the edge fluxes. It now remains to define an appropriate gradient $\vec{L}$ for the linear reconstruction of the solution within each cell of the grid.

A simple gradient operator which is exact for linear data can be defined on any grid by taking the (constant) solution value in three arbitrarily chosen, but preferably adjacent, cells (i, j and k say, forming a triangle with anticlockwise indexing of its vertices) and defining

$$\vec{\nabla}(\triangle ijk) \;=\; \begin{cases} \begin{pmatrix} -\frac{n_x}{n_u} \\ -\frac{n_y}{n_u} \end{pmatrix} & \text{for} \quad n_u \geq \epsilon \\ \begin{pmatrix} 0 \\ 0 \end{pmatrix} & \text{otherwise} \;, \end{cases} \tag{2.10}$$

in which $\epsilon \approx 10^{-10}$ and n_x, n_y and n_u are the components of the vector $\mathbf{n}$ normal to the plane defined by the triangle ijk in xyu-space given by

$$\mathbf{n} \;=\; (\underline{P}_i - \underline{P}_k) \times (\underline{P}_j - \underline{P}_k) \;, \tag{2.11}$$

where

$$\underline{P}_* \;=\; \begin{pmatrix} \\ \\ \end{pmatrix} \qquad \geq 1) \qquad \text{whe} \quad \text{r} \quad \text{normae gihas dwhieesolutionTre lo}$$

deal with the possibility of $\triangle ijk$ having a non-positive area. An example of such a triangle is shaded in Figure 2.3.

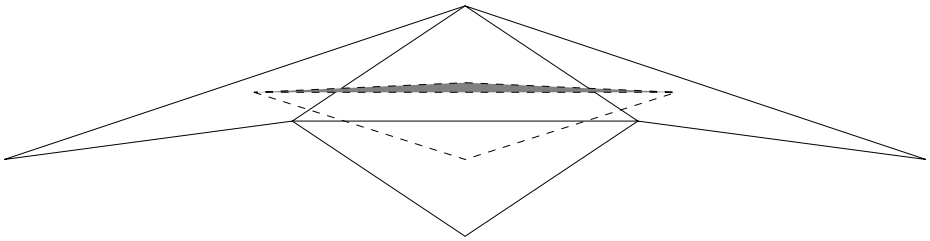

The Maximum Limited Gradient (MLG) scheme devised by Batten *et al.* [2] improves on the LCD scheme by using the ideas of Durlofsky *et al.* [3] to create a far more compressive limiter. The MLG scheme chooses its initial reconstruction from the four gradient operators

$$\vec{\nabla}(\triangle 123)\ ,\quad \vec{\nabla}(\triangle 023)\ ,\quad \vec{\nabla}(\triangle 103)\ ,\quad \vec{\nabla}(\triangle 120)$$

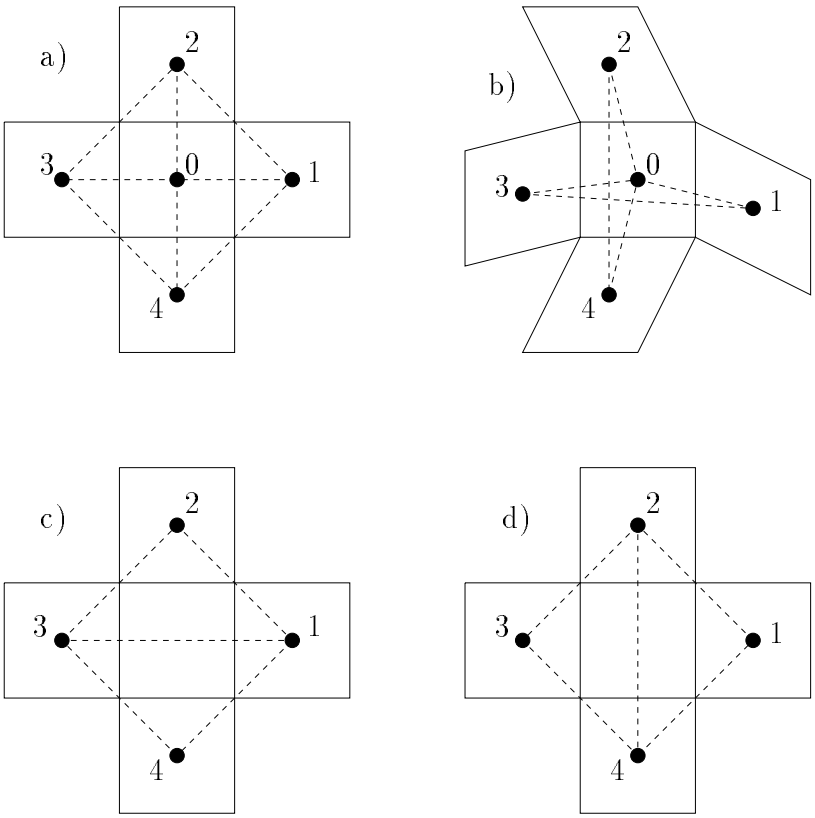

Figure 2.4: The limiting planes as defined for a quadrilateral control volume.

selection of the gradient operators, *cf.* (2.14) and (2.15) in the first step of the limiting. A grid cell now has four edge-neighbours and hence ten possible choices for the gradient operator (all shown in Figure 2.4). For the sake of computational speed not all of these operators would be considered. In particular, the two triangles in Figure 2.4b) hav

- Maximise $f(x, y) =$

The DS limiter is similar in many ways to the slope limiters described above, and the multidimensional gradient operators can be modified and limited so that the resulting scheme is equivalent on rectangular grids. The gradient operators are decoupled into components in the two grid directions and a separate value of α is calculated in the manner of (2.13) (taking into account only the constraints in the relevant grid directions) for each of the components, so

$$\vec{L} \;=\; \begin{pmatrix} \alpha_x L_x \\ \alpha_y L_y \end{pmatrix} . \tag{2.22}$$

The MLG-type limiting procedure calculates a single value of α which satisfies

$$\alpha \;=\; \min(\alpha_x, \alpha_y) \tag{2.23}$$

and is therefore far less compressive.

The type of modification given by (2.22) cannot be applied on grids where successive cell centroids do not lie in a straight line, but then the DS approac

In both of the above limits the maximum is taken over the adjacent cells.

The global time-step restriction used with the DS limited scheme is defined to be

$$\Delta t \leq \min_{i,j} \frac{|\vec{x}_{ij}|}{2\left(c + \sqrt{u^2 + v^2}\right)_{ij}} , \tag{2.28}$$

where $\vec{x}_{ij}$ is the vector joining the centroid of cell i to the centroid of cell j, an edge-neighbour of cell i.

2.5 Results

Numerical experiments have been carried out to test the behaviour of all of the schemes described in this report. The first test presented here is the advection of an initial profile given by the double sine wave function

$$u \;=\; \sin(2\pi x)\sin(2\pi y) , \tag{2.29}$$

with velocity $\vec{\lambda} = (1, 1)^T$ over the domain $[0, 1] \times [0, 1]$. This problem has been solved on three types of grid each of which is illustrated in Figure 2.6. Periodic boundary conditions are applied.

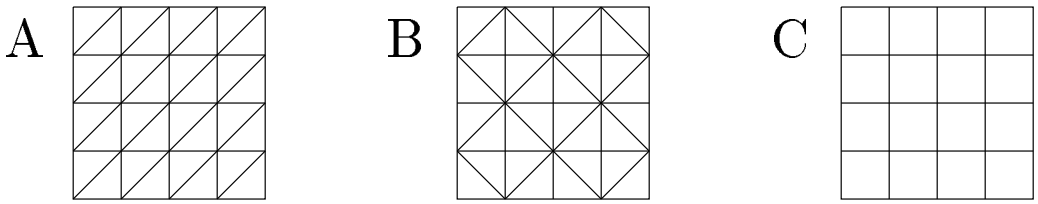

Figure 2.6: The three grid types used for the numerical experiments.

Error estimates in the L_2 norm for the solution when $t = 0.1$ are shown in Figure 2.7. The errors in the L_1 and L_∞ norms behave in a similar manner for all of the grids used. In all of the numerical experiments the ratio $dt/dx = 0.04$ where dx is the length of any horizontal grid edge in Figure 2.6. The first order scheme is unsurprisingly the least accurate. Of the second order schemes the MLG limiter gives easily the most accurate results on grid A and is the only one of the schemes on triangles that approaches second order accuracy (roughly 1.88 at the finest grid level), better even than the dimensionally split quadrilateral scheme for which errors are also shown in the figure. It should be noted that for

a precise comparison in terms of computational effort (*i.e.* number of cells rather than grid size) the graph for the quadrilateral grid should be shifted 0.15 to the right. Even then the MLG scheme is better. On the coarsest grid the GI scheme is best but it rapidly deteriorates until it is only slightly more accurate than the LCD scheme.

On grid B all of the linear reconstruction schemes on triangles give considerably worse results than on grid A, in particular the MLG scheme, which is now the worst on the finest grids. It is now the GI scheme which is the most accurate, although the results are nowhere near the quality of those obtained on the quadrilateral grids.

The advantage of using the GI scheme is clarified by considering a second test case. It in

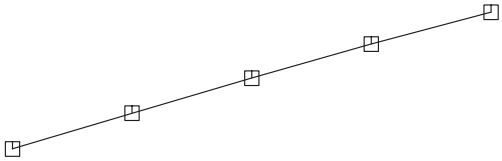

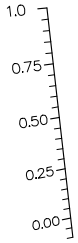
1.0
0.75
0.50
0.25
0.00

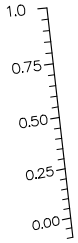
1.0
0.75
0.50
0.25
0.00

Scheme	L_1	L_2	L_∞	Peak value	Time (s)
First order	0.0152	0.0621	0.7161	0.284	94
LCD	0.0094	0.0431	0.5358	0.479	120
MLG	0.0055	0.0281	0.3855	0.617	154
GI	0.0029	0.0152	0.2009	0.887	11%%%%%Tm2154Tj2ET2q2%%

by Roe [7]. The evolution of the discontinuous approximation to the solution is modelled by constructing a series of approximate Riemann problems at the edge midpoints with left and right states $\underline{U}_L$ and $\underline{U}_R$ respectively (the internal and external states relative to the control volume). Each Riemann problem is solved by decomposing the flux difference across the edge into its characteristic components, which results in a numerical flux function for edge k given by

$$(\underline{F}^*(\underline{U}_L, \underline{U}_R), \underline{G}^*(\underline{U}_L, \underline{U}_R)) \cdot \vec{n}_k \;=\; \tfrac{1}{2}\,((\underline{F}_L, \underline{G}$$

so the limiti

pletely by the imposed solution values, (b) supercritical outflow, where no eigenvalue is positive and the flux is calculated from internal solution values, (c) subcritical inflow, where one eigenvalue is negative whose corresponding Riemann invariant is given its internal value and everything else is imposed, and finally

25

25
5

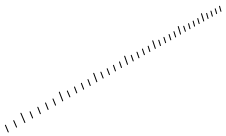

wave front reached the corner. The agreement with experimental data is good for both schemes at P1. At P2 the reflected wave fron

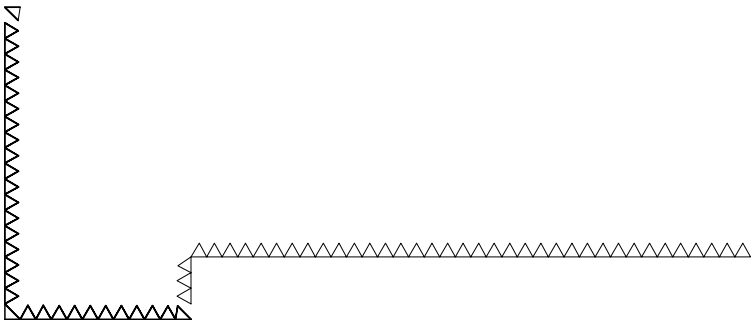

briefly.

It has been shown that the family of monotonicity enforcing limiters can be completely defined by constraints applied at the midpoints of the edges of the cells. These constraints define a region within which every valid limiter lies. Furthermore, it follows that a limiter can be constructed which gives the maximum possible slope for the reconstruction. It has the property of removing the dependence of the reconstruction on the geometry of the surrounding grid cells but, although it is considerably cheaper than the most accurate of the previously constructed limiters and preserves peaks far better, the general quality of the solutions is worse. However, given the monotonicity region it should be possible tola monrerccuratelimiter

[5] C.Hirsch, *Fundamentals of Numerical iscretization*, volume 1 of *Numerical omputation of Internal and External Flows*, Wiley, 1990.

[6] M.E.Hubbard and M.J.Baines, 'Conservative multidimensional upwinding for the steady two-dimensional shallow water equations', To appear, *J. omput. Phys.*, 1997.

[7] P.L.Roe, 'Approximate Riemann Solvers, parameter vectors, and difference schemes', *J. omput. Phys.*, **43(2)**:357–372, 1981.

[8] P.K.Sweby, 'High resolution schemes using flux limiters for hyperbolic conservation laws', *IAM J. Numer. Anal.*, **21**:995–1011, 1984.

[9] B.van Leer, 'Towards the ultimate conservative difference scheme V. A second order sequel to Godunov's method', *J. omput. Phys.*, **32**:101–136, 1979.

[10] B.van Leer, 'On the relation between the upwind-differencing schemes of Godunov, Engquist-Osher and Roe', *IAM J. cientific tatist. omput.*, **5**, 1984.

[11] P.R.Woodward and P.Collela, 'The numerical simulation of two-dimensional fluid flow with strong shocks', *J. omput. Phys.*, **54**:115–173, 1984.

A The Sh llow W ter Equ tions

The shallow water equations depend on the conservative variables and fluxes given by

$$\underline{U} = \begin{pmatrix} h \\ hu \\ hv \end{pmatrix}, \quad \underline{F} = \begin{pmatrix} hu \\ hu^2 + \frac{gh^2}{2} \\ huv \end{pmatrix}, \quad \underline{G} = \begin{pmatrix} hv \\ huv \\ hv^2 + \frac{gh^2}{2} \end{pmatrix}, \qquad \text{(A.1)}$$

where h is the depth of the flow, u and v are the x- and y-velocities and g is the acceleration due to gravity, and result in the following flux Jacobians:

$$\mathbf{A} = \frac{\partial \underline{F}}{\partial \underline{U}} = \begin{pmatrix} 0 & 1 \\ & \end{pmatrix}$$

where $c = \sqrt{gh}$ is the gravity wave speed.

In Roe's approximate Riemann solver the eigenvalues and eigenvectors of the matrix

($\mathbf{A}$, $\mathbf{B}$

B The Euler Equations

The Euler equations depend on the conservative variables and fluxes given by

$$\underline{U} = \begin{pmatrix} \rho \\ \rho u \\ \rho v \\ e \end{pmatrix}, \quad \underline{F} = \begin{pmatrix} \rho u \\ p + \rho u^2 \\ \rho uv \\ u(e+p) \end{pmatrix}, \quad \underline{G} = \begin{pmatrix} \rho v \\ \rho uv \\ p + \rho v^2 \\ v(e+p) \end{pmatrix}, \tag{B.1}$$

where ρ is the density of the flow, u and v are the x- and y-velocities, p is pressure and e is the total energy, related to the other variables by an equation of state which, for a perfect gas, is

$$e = \frac{p}{\gamma - 1} + \frac{1}{2}\rho(u^2 + v^2) , \tag{B.2}$$

and result in the following flux Jacobians:

$$\mathbf{A} = \frac{\partial \underline{F}}{\partial \underline{U}} = \begin{pmatrix} 0 & 1 & 0 & 0 \\ \frac{\gamma-1}{2}(u^2+v^2) - u^2 & (3-\gamma)u & (1-\gamma)v & \gamma - 1 \\ -uv & v & u & 0 \\ \frac{\gamma-1}{2}u(u^2+v^2) - uH & u^2(1-\gamma) + H & (1-\gamma)uv & \gamma u \end{pmatrix} \tag{B.3}$$

and

$$\mathbf{B} = \frac{\partial \underline{G}}{\partial \underline{U}} = \begin{pmatrix} 0 & 0 & 1 & 0 \\ -uv & v & u & 0 \\ \frac{\gamma-1}{2}(u^2+v^2) - v^2 & (1-\gamma)u & (3-\gamma)v & \gamma - 1 \\ \frac{\gamma-1}{2}v(u^2+v^2) - vH & (1-\gamma)uv & v^2(1-\gamma) + H & \gamma v \end{pmatrix}, \tag{B.4}$$

where $H = \frac{\gamma e}{\rho} - \frac{\gamma-1}{2}(u^2+v^2)$ is the total enthalpy.

In Roe's approximate Riemann solver the eigenvalues and eigenvectors of the matrix

$$(\mathbf{A}, \mathbf{B}) \cdot \vec{n} = \mathbf{A}n_x + \mathbf{B}n_y \tag{B.5}$$

are

$$\begin{aligned} \lambda_1 &= \tilde{u}n_x + \tilde{v}n_y + \tilde{c} , \quad \lambda_2 = \tilde{u}n_x + \tilde{v}n_y , \\ \lambda_3 &= \tilde{u}n_x + \tilde{v}n_y , \quad \lambda_4 = \tilde{u}n_x + \tilde{v}n_y - \tilde{c} , \end{aligned} \tag{B.6}$$

and

$$\underline{r}_1 = \frac{\tilde{\rho}}{2\tilde{c}} \begin{pmatrix} 1 \\ \tilde{u} + \tilde{c}n_x \\ \tilde{v} + \tilde{c}n_y \\ \tilde{H} + \tilde{c}(\tilde{u}n_x + \tilde{v}n_y) \end{pmatrix}, \quad \underline{r}_2 = \tilde{\rho} \begin{pmatrix} 0 \\ -n_y \\ n_x \\ -\tilde{u}n_y + \tilde{v}n_x \end{pmatrix},$$

$$\underline{r}_3 = \begin{pmatrix} 1 \\ \tilde{u} \\ \tilde{v} \\ \frac{1}{2}(\tilde{u}^2 + \tilde{v}^2) \end{pmatrix}, \quad \underline{r}_4 = \frac{\tilde{\rho}}{2\tilde{c}} \begin{pmatrix} 1 \\ \tilde{u} - \tilde{c}n_x \\ \tilde{v} - \tilde{c}n_y \\ \tilde{H} - \tilde{c}(\tilde{u}n_x + \tilde{v}n_y) \end{pmatrix}, \tag{B.7}$$

respectively, and the corresponding wave strengths in (3.5) are given by $\alpha_j = \Delta W_j$ for $j = 1, 2, 3, 4$, where

$$\Delta \underline{W} = \mathbf{L} \Delta \underline{U} \tag{B.8}$$

and

$$\mathbf{L} = \begin{pmatrix} -\frac{\tilde{u}n_x + \tilde{v}n_y}{\tilde{\rho}} + \frac{(\gamma-1)(\tilde{u}^2+\tilde{v}^2)}{2\tilde{\rho}\tilde{c}} & \frac{n_x}{\tilde{\rho}} - \frac{(\gamma-1)\tilde{u}}{\tilde{\rho}\tilde{c}} & \frac{n_y}{\tilde{\rho}} - \frac{(\gamma-1)\tilde{v}}{\tilde{\rho}\tilde{c}} & \frac{(\gamma-1)}{\tilde{\rho}\tilde{c}} \\ \frac{\tilde{u}n_y - \tilde{v}n_x}{\tilde{\rho}} & -\frac{n_y}{\tilde{\rho}} & \frac{n_x}{\tilde{\rho}} & 0 \\ 1 - \frac{(\gamma-1)(\tilde{u}^2+\tilde{v}^2)}{2\tilde{c}^2} & \frac{(\gamma-1)\tilde{u}}{\tilde{c}^2} & \frac{(\gamma-1)\tilde{v}}{\tilde{c}^2} & -\frac{(\gamma-1)}{\tilde{c}^2} \\ \frac{\tilde{u}n_x + \tilde{v}n_y}{\tilde{\rho}} + \frac{(\gamma-1)(\tilde{u}^2+\tilde{v}^2)}{2\tilde{\rho}\tilde{c}} & -\frac{n_x}{\tilde{\rho}} - \frac{(\gamma-1)\tilde{u}}{\tilde{\rho}\tilde{c}} & -\frac{n_y}{\tilde{\rho}} - \frac{(\gamma-1)\tilde{v}}{\tilde{\rho}\tilde{c}} & \frac{(\gamma-1)}{\tilde{\rho}\tilde{c}} \end{pmatrix}. \tag{B.9}$$

The Roe averages $\tilde{u}$, $\tilde{v}$, $\tilde{c}$ and $\tilde{H}$ are evaluated consistently from the average values of the parameter vector variables given by

$$\underline{\tilde{Z}} = \frac{1}{2}(\underline{Z}_L + \underline{Z}_R), \tag{B.10}$$

where

$$\underline{Z} = \sqrt{\rho} \begin{pmatrix} 1 \\ u \\ v \\ H \end{pmatrix}. \tag{B.11}$$